

indicating that composition of the B2 phase obtained in our experiments is close to 1:1 Fe:Si molar ratio.

As mentioned above, the Fe-4.3(4) wt% Si alloy, obtained by reacting SiO₂ and Fe at 22 GPa and 2,473 K in a multianvil apparatus, was homogeneous. However, ATEM studies of the material recovered after treatment of this alloy in a laser-heated DAC at 93(3) GPa and 2,100–2,400 K reveal a variation of silicon concentrations in different parts of the sample from ~0 to 6.6 wt%. These observations provide direct proof that the Fe–Si alloy, equilibrated with SiO₂ at relatively low pressures (20–30 GPa), dissociates into Si-poor and Si-rich phases at much higher pressures (about 100 GPa).

Our results on the behaviour of the Fe–Si alloys with different Si concentrations are summarized in Fig. 2b. We found that at pressures above 60 GPa and high temperatures the alloys dissociate into a mixture of h.c.p.-structured Si-poor and B2-structured Si-rich phases. Lin *et al.*¹⁷ also reported dissociation of Fe–Si alloys with a Si content of more than 4 wt% on the mixture of h.c.p. and b.c.c. phases. The difference between b.c.c.- and B2-structured alloys is solely the ordering of Fe/Si atoms among the positions in the body-centred lattice—fully or partially ordered alloys are B2, and completely disordered alloys are b.c.c. Our diffraction data clearly show the (100) reflection of the B2 structure (Fig. 3d and insets), which is expected to be low in intensity (calculated intensity is 14% for a fully ordered stoichiometric FeSi compound), and could be rather difficult to detect in high pressure and temperature experiments.

The reaction between iron and silicate^{2,9,10,13} could be a source of the iron–silicon alloy at the CMB. The density of B2 FeSi (~9.0 g cm⁻³) is significantly higher than the density of the mantle (~5.6 g cm⁻³) above the CMB and lower than the density of the core (~10.0 g cm⁻³) immediately below the CMB. This means that the silicon-rich alloy would accumulate at the boundary between mantle and core. *Ab initio* simulations (see Supplementary Information) and measurements on B2 FeSi recovered from multianvil experiments¹⁹ show that this compound is an electric conductor (with the electrical conductivity of 6(1) × 10⁵ S m⁻¹ measured at ambient conditions). Thus, anomalously high electrical conductivity at the base of Earth's mantle⁶ could be associated with the presence of B2 FeSi.

We suggest that if silicon is present in the inner core, it should form a B2 FeSi phase (assuming that there are no further phase transitions in this material above 300 GPa and high temperatures). This implies that the Earth's inner core can be compositionally heterogeneous and contains at least two phases—the Fe-rich phase with hexagonal symmetry and the Fe–Si phase with cubic symmetry. The elastic and rheological properties of these two phases are expected to be quite different and could influence the understanding of the observed inner core anisotropy and heterogeneity^{5,6,11,16,17}. □

Received 28 May 2002; accepted 8 January 2003; doi:10.1038/nature01422.

- Gurnis, M., Wyssession, M. E. & Knittle, E. *The Core-Mantle Boundary Region* (ed. Buffett, B. A.) (AGU, Washington DC, 1998).
- Jeanloz, R. & Williams, Q. in *Ultrahigh-Pressure Mineralogy: Physics and Chemistry of the Earth's Deep Interior* (ed. Hemley, R. J.) *Rev. Mineral.*, **37**, 241–259 (1998).
- Buffett, B. A., Garner, E. J. & Jeanloz, R. Sediments at the top of Earth's core. *Science* **290**, 1338–1342 (2000).
- Li, J. & Agee, C. B. Geochemistry of mantle–core differentiation at high pressure. *Nature* **381**, 686–689 (1996).
- Vidale, J. E. & Earle, P. S. Fine-scale heterogeneity in the Earth's inner core. *Nature* **404**, 273–275 (2001).
- Buffett, B. A. Constraints on magnetic energy and mantle conductivity from the forced nutations of the Earth. *J. Geophys. Res.* **97**, 19581–19597 (1992).
- Carnero, E. J. & Jeanloz, R. Fuzzy patches on the Earth's core-mantle boundary? *Geophys. Res. Lett.* **27**, 2777–2780 (2000).
- Gessmann, C. K., Wood, B. J., Rubie, D. C. & Kilburn, M. R. Solubility of silicon in liquid metal at high pressure: implications for the composition of the Earth's core. *Earth Planet. Sci. Lett.* **184**, 367–376 (2001).
- Knittle, E. & Jeanloz, R. Simulating the core-mantle boundary: an experimental study of high-pressure reactions between silicates and liquid iron. *Geophys. Res. Lett.* **16**, 609–612 (1989).
- Poirier, J. P., Malavergne, V. & Le Mouél, J. L. in *The Core-Mantle Boundary Region* (eds Gurnis, M., Wyssession, M. E., Knittle, E. & Buffett, B. A.) 131–137 (AGU, Washington DC, 1998).

- Steinle-Neumann, G., Stixrude, L., Cohen, R. E. & Gulseren, O. Elasticity of iron at the temperature of the Earth's inner core. *Nature* **413**, 57–60 (2001).
- Goarant, F., Guyot, F., Peyroneau, J. & Poirier, J. P. High-pressure and high-temperature reactions between silicates and liquid iron alloys in the diamond anvil cell, studied by analytical electron microscopy. *J. Geophys. Res.* **97**, 4477–4487 (1992).
- Song, X. & Ahrens, T. J. Pressure-temperature range of reactions between liquid iron in the outer core and mantle silicates. *Geophys. Res. Lett.* **21**, 153–156 (1994).
- Tschauner, O., Zerr, A., Specht, S., Rocholl, A., Boehler, R. & Palme, H. Partitioning of nickel and cobalt between silicate perovskite and metal at pressures up to 80 GPa. *Nature* **398**, 604–607 (1999).
- Dubrovinsky, L. *et al.* Chemical interaction of iron and corundum as a source of heterogeneity at the core-mantle boundary. *Nature* **412**, 527–529 (2001).
- Dubrovinsky, L. S., Saxena, S. K., Tutti, F. & Le Bihan, T. X-ray study of thermal expansion and phase transition of iron at multimegabar pressure. *Phys. Rev. Lett.* **84**, 1720–1723 (2000).
- Lin, J.-F., Heinz, D. L., Campbell, A. J., Devine, J. M. & Shen, G. Iron-silicon alloy in Earth's core? *Science* **295**, 313–315 (2002).
- Knittle, E. & Jeanloz, R. Earth's core-mantle boundary: Results of experiments at high pressures and high temperatures. *Science* **251**, 1438–1443 (1991).
- Dobson, D. P., Vocadlo, L. & Wood, I. G. A new high-pressure phase of FeSi. *Am. Mineral.* (in the press).
- Prokopenko, V. B., Dubrovinsky, L. S., Dmitriev, V. & Weber, H.-P. Raman spectroscopy and X-ray diffraction *in situ* characterization of phase transitions in cristobalite under high pressure. *J. Alloys Compounds* **327**, 87–95 (2001).
- Guyot, F. *et al.* P-V-T measurements of iron silicide (ε-FeSi)—Implications for silicate-iron interactions in the early Earth. *Eur. J. Mineral.* **9**, 277–285 (1997).
- Alfe, D., Price, G. D. & Gillan, M. J. Thermodynamic stability of Fe/O solid solution at inner-core conditions. *Geophys. Res. Lett.* **27**, 2417–2420 (2000).
- Boehler, R. Temperatures in the Earth's core from melting-point measurements of iron at high static pressures. *Nature* **363**, 534–536 (1993).
- Shen, G., Mao, H. K., Hemley, R. J. & Rievers, M. L. Melting and crystal structure of iron at high pressure. *Geophys. Res. Lett.* **25**, 373–376 (1998).

Supplementary Information accompanies the paper on Nature's website (<http://www.nature.com/nature>).

Acknowledgements We thank G. Herrmannsdörfer, H. Schulze, R. Eger and C. Kamella, for technical assistance. Discussion with G. D. Price allowed us to improve the manuscript. Financial support of Deutsche Forschungsgemeinschaft, the Swedish Research Council (VR), the Swedish Foundation for Strategic Research (SSF), and the EU 'Access to Research Infrastructures' Programme is acknowledged.

Competing interests statement The authors declare that they have no competing financial interests.

Correspondence and requests for materials should be addressed to L.D. (e-mail: Leonid.Dubrovinsky@uni-bayreuth.de).

A Middle Miocene hominoid from Thailand and orangutan origins

Yaowalak Chaimanee*, Dominique Jolly†, Mouloud Benammi‡, Paul Tafforeau§, Danielle Duzer†, Issam Moussa§ & Jean-Jacques Jaeger§

* Paleontology Section, Geological Survey Division, Department of Mineral Resources, Bangkok -10400, Thailand

† Palynologie et Paléoenvironnements, I.S.E.M., cc 061, Place Eugene Bataillon, 34095-Montpellier, France

‡ Paleomagnetismo, Instituto de Geofísica, Universidad Nacional Autónoma de México, 04510 México DF, México

§ Paléontologie, I.S.E.M., cc 064, Université Montpellier II, Place Eugene Bataillon, 34095-Montpellier, France

The origin of orangutans has long been debated. *Sivapithecus* is considered to be the closest ancestor of orangutans because of its facial–palatal similarities¹, but its dental characteristics² and postcranial skeleton^{2,3} do not confirm this phylogenetic position. Here we report a new Middle Miocene hominoid, cf. *Lufengpithecus chiangmuanensis* n. sp. from northern Thailand. Its dental morphology relates it to the *Pongo* clade, which includes *Lufengpithecus*^{4,5}, *Sivapithecus*², *Gigantopithecus*⁶, *Ankarapithecus*⁷ and possibly *Griphopithecus*⁸. Our new species

displays striking dental resemblances with living orangutans and appears as a more likely candidate to represent an ancestor of this ape. In addition, it originates from the geographic area of Pleistocene orangutans. But surprisingly, the associated flora shows strong African affinities, demonstrating the existence of a temporary floral and faunal dispersal corridor between south-east Asia and Africa during the Middle Miocene, which may have played a critical role in hominoid dispersion.

The new hominoid remains were recovered from the middle and upper lignite seams of Ban Sa locality, Chiang Muan basin, northern Thailand. The sediments consist mainly of mudstones and sandstones intercalated with palaeosols and several lignite beds. Associated large mammals are similar to those of the Chinji Formation of Pakistan, dated between 14 and 10.8 million years (Myr)⁹. Palaeomagnetic data indicate two normal events sandwiching a reverse polarity zone, the hominoid originating from the upper normal zone (Fig. 1). Our age estimation, between 13.5 and 10 Myr, is congruent with the absence of C4 plants, which appear around 10 Myr in the Siwaliks¹⁰ and become abundant about 8–7 Myr¹¹. Enamel of several ungulates shows ¹²C/¹³C isotopic ratios ($\delta^{13}C$ values) of -13.4 to -11.8‰ (Pee Dee belemnite standard), demonstrating a diet exclusively based on C3 plants¹⁰. Palaeosols indicate some climatic seasonality, which is confirmed by palynology from the lignites. The vegetation corresponded to a mosaic of tropical freshwater swamps, with a *Syzygium*-dominated lowland forest (Fig. 2), similar to an extant African habitat from the White Nile headwaters¹², but differing from the temperate Late Miocene Lufeng flora of southern China¹³. This resemblance with African flora testifies to the existence, in the Middle Miocene, of a dispersal corridor between southeast Asia and Africa, the duration and location of which have yet to be precisely determined.

Order Primates Linnaeus, 1758
 Suborder Anthroidea Mivart, 1864
 Superfamily Hominoidea Gray, 1825
 Family Hominidae Gray, 1825
 Subfamily Ponginae Elliot, 1913
cf. Lufengpithecus chiangmuanensis sp. nov.

Etymology. The species is named according to the type locality.

Holotype. Right lower canine fragment (TF 6171-1), left P₃ fragment (TF 6171-2), right P₄ (TF 6171-3), right M₂ (TF 6171-4), left M₂₋₃ (TF 6171-5, 6171-6) (Fig. 3 c–f, h) and right P₃ fragment (TF 6171-7) (Department of Mineral Resources, Bangkok).

Referred materials. Right I¹ (TF 6168), right M² (TF 6169), left dP₄ (TF 6170) (Fig. 3 a, b, g). Left upper canine (TF 6174), right I² (TF 6173), left I₁ (TF 6178), right P³ (TF 6175), left M²⁻³ (TF 6176, 6177), left P₄ (TF 6179) and right M₂ (TF 6180) (Fig. 3 i–o) and right M₃ fragment (TF 6172).

Horizon and locality. Middle and upper lignite seams of Chiang Muan Basin, Ban Sa locality, northern Thailand, Middle Miocene age.

Diagnosis. Large hominoid with dental size and jugal teeth morphology, wear patterns, crown elevation, enamel thickness and wrinkling, apparent strong sexual dimorphism, similar to *Lufengpithecus lufengensis* Wu 1987, from which it differs by its anterior dentition, greater mesio-distal length and lower elevation of its lower central incisor crowns with more divergent mesial and distal margins, rounded lower canine crown section and less heteromorphic P³, P₃ without metaconid, more slanted P₃ and P₄ buccal cusps and M₃ larger than M₂. Differs from *Sivapithecus* by less lingually flared upper molar crowns, more nearly square molar occlusal surfaces, higher molar cusps, dentine horns with greater

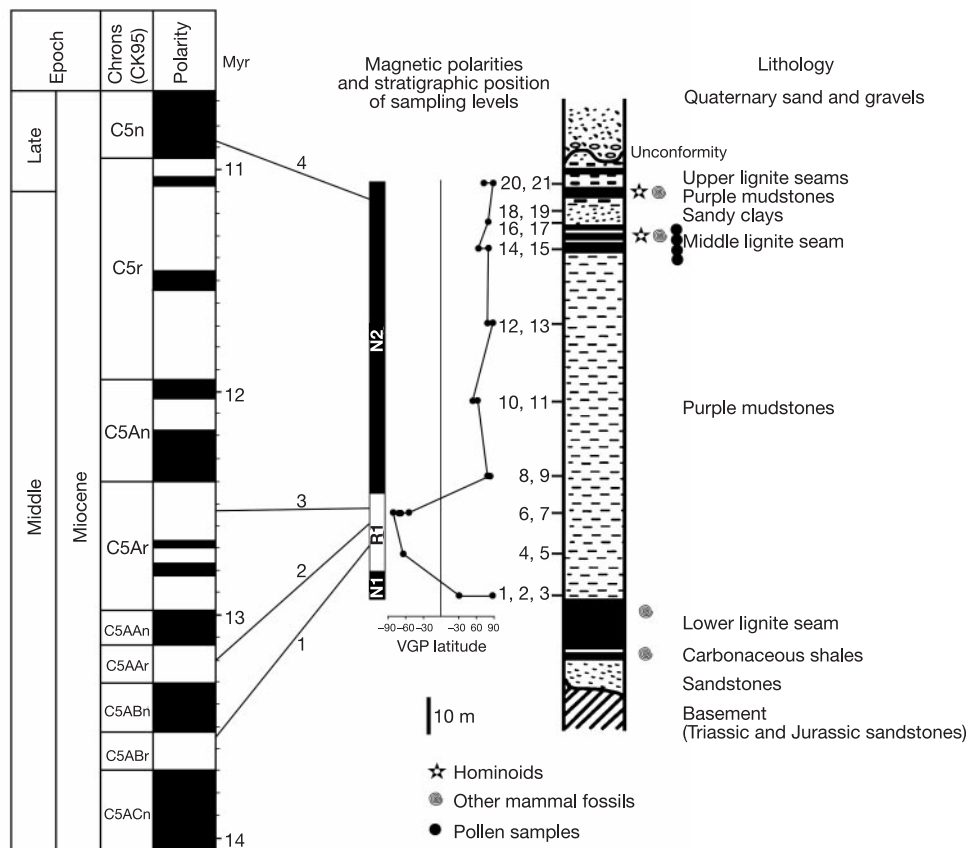


Figure 1 Stratigraphic section of Ban Sa coalmine bearing *cf. Lufengpithecus chiangmuanensis*. Lines (1–4) indicate four possible correlations with the magnetic polarity timescale (see Methods).

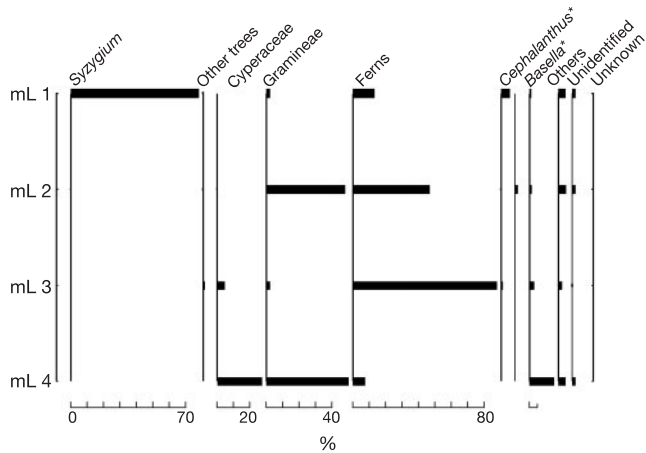


Figure 2 Simplified pollen diagram of four samples collected from the middle lignite seam in Ban Sa section. The pollen spectra (268–1040 identified pollen grains counted in each sample) are characterized by a high taxonomic diversity (30 taxa). *Syzygium* forest dominates at the level that has yielded most hominoid remains (mL1). 'Other trees' includes *Alchornea*, *Celtis*, *Macaranga*, *Murraya*, Meliaceae, Mimosaceae, *Pometia*, Rutaceae and Moraceae. 'Others' includes Rubiaceae, Apiaceae, Celastraceae, Compositae, *Polygonum*, Combretaceae, *Merremia*, *Elitranthe*, Malpighiaceae, Papilionoideae, Euphorbiaceae, *Lasianthus* and Eleagnaceae. The presence of *Cephalanthus*, a deciduous wetland shrub, associated with *Celtis*, Mimosaceae and some Combretaceae, implies a dry-season climate.

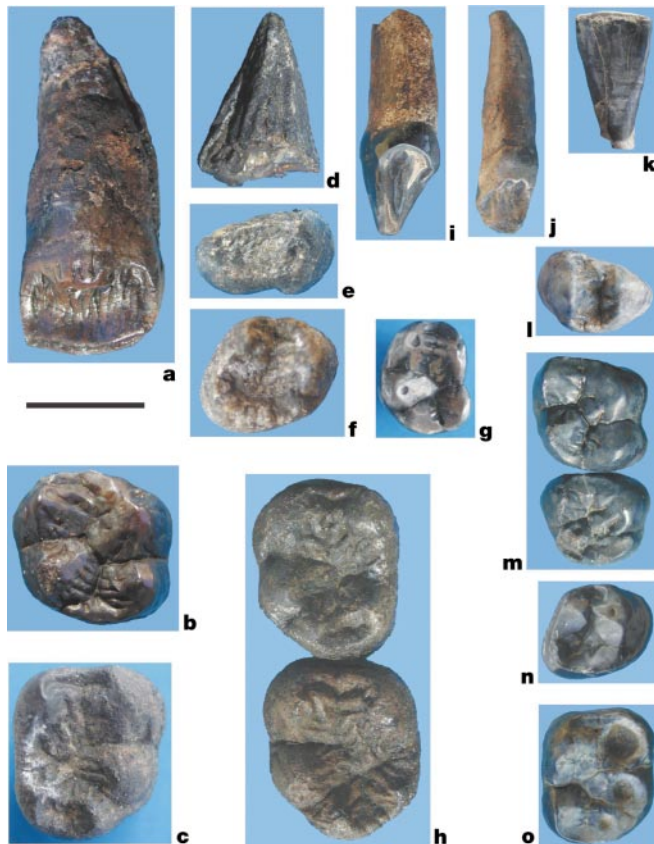


Figure 3 cf. *Lufengpithecus chiangmuanensis* n. sp. **a**, TF 6168, right I¹. **b**, TF 6169, right M². **c**, TF 6171-4, right M₂₋₃. **d**, TF 6171-1, right lower canine. **e**, TF 6171-2, distal part of left P₃ (mirror image). **f**, TF 6171-3, right P₄. **g**, TF 6170, left dP₄. **h**, TF 6171-5, 6171-6, left M₂₋₃. **i**, TF 6174, left upper canine. **j**, TF 6173, right I². **k**, TF 6178, left I₁. **l**, TF 6175, right P³. **m**, TF 6176, 6177, left M²⁻³ (mirror image). **n**, TF 6179, left P₄ (mirror image). **o**, TF 6180, right M₂. Scale bar, 1 cm.

relief and by different morphology of its I¹, I², canine and P³. Differs from *Ankarapithecus* by its larger upper central incisors, smaller P³ and M₃ larger than M₂. Differs from *Griphopithecus* by its larger size and more wrinkled enamel, larger I¹ with different root/crown proportions, less heteromorphic P³ with stronger lingual flaring, molars with more elevated crowns, I₁ with more divergent mesial and distal margins, P₃ without strong beaks and M₃ larger than M₂, without cingulids. Differs from *Pongo* by its less peripheralized and more flared upper lingual and lower buccal molar cusps and greater molar occlusal relief, smaller lower incisors but with similar length/breadth index, less heteromorphic P³ with low and slanted protocone and less densely crenulated enamel. Differs from *Ouranopithecus* by its anterior dentition, less enlarged M₃ and much thinner enamel. Differs from *Dryopithecus* by its thicker enamel, incisors size, absence of cingula, wider lower molars, and smaller P₃.

The holotype teeth belonged to a single individual. Main characters (wrinkled enamel, very large I¹, small and peg-like I², low crowned P³ with reduced heteromorphy, absence of molar cingula) indicate that it belongs to the *Pongo* clade, represented by *Lufengpithecus* (10–3 Myr) (ref. 5), *Sivapithecus* (12.3–8.5 Myr) (ref. 9), *Gigantopithecus* (7–6 Myr), *Ankarapithecus* (9.89–9.59 Myr)⁷ and Pleistocene to extant *Pongo*¹⁴. Two size categories are represented in our samples (Table 1), which, according to the morphological similarities, are interpreted as presumed male and female, as for *L. lufengensis*¹⁵.

I¹ is similar in crown proportions and size to the largest I¹'s of *S. sivalensis* (bucco-lingual breadth/mesio-distal length, 0.77; labial height/mesio-distal length, 0.95) (ref. 16), but its crown, root morphology and root/crown proportions are more similar to *L. lufengensis* (J. Kelley, personal communication). It also resembles *Pongo*, differing by its smaller size, the absence of a strong central lingual pillar and by having fewer vertical lingual ridges. I² is small and peg-shaped, with an asymmetric crown and spiral lingual cingulum, differing from *Pongo* by the absence of a strong central lingual pillar and by stronger asymmetry. Female upper canine is small and low-crowned. It shows weak cervical flare and a well-developed basal lingual cingulum connecting the mesial and distal ridges. P³ has an asymmetric triangular occlusal outline, without cingula and with an extended mesio-buccal corner. Heteromorphy is reduced and the lingual crown surface is strongly flaring. The small-sized M² and M³ share many similarities with those of *L. lufengensis*, differing by their more slanted buccal cusps. M³ is reduced, especially its distal half with a more curving buccal wall than that of M². The anterior fovea is absent and the paracone is

Table 1 Dental measurements (in millimetres) of cf. *Lufengpithecus chiangmuanensis* n. sp. Holotype (TF 6171)

Presumed male		MD	BL	
I ¹ R	(TF 6168)	11.97	8.87	
M ² R	(TF 6169)	12.64	13.48	
		MD	BL (trd.)	(tad.)
dP ₄ L	(TF 6170)	9.92	8.07	
C _R	(TF 6171-1)	10.59	10.54	
P ₃ L	(TF 6171-2)	—	> 8.00	
P ₃ R	(TF 6171-7)	> 12.00	8.55	
P ₄ R	(TF 6171-3)	10.32	10.97	
M ₂ R	(TF 6171-4)	14.38	12.75	11.60
M ₂ L	(TF 6171-5)	13.97	11.76	10.80
M ₃ L	(TF 6171-6)	15.79	12.79	11.80
M ₃ R	(TF 6172)	—	12.70	
Presumed female				
I ² R	(TF 6173)	5.08	4.61	
C ^L	(TF 6174)	9.09	8.54	
P ³ R	(TF 6175)	7.17	9.94	
M ² L	(TF 6176)	9.95	10.42	
M ³ L	(TF 6177)	8.85	10.17	
I ₁ L	(TF 6178)	5.07	5.26	
P ₄ L	(TF 6179)	8.66	7.89	
M ₂ R	(TF 6180)	11.56	9.41	

MD, mesiodistal; BL, buccolingual; trd., trigonid; tad. talonid; R, right; L, left.

more slanted. The male M^2 is larger, strongly wrinkled, but shares the same morphology as the smaller M^2 . I_1 occlusal surface is rather long mesio-distally, its crown is relatively low and the mesial and distal tooth margins are divergent rather than parallel as those of *L. lufengensis*. Only a tiny central rib can be distinguished on its lingual side and there are neither marginal ridges nor lingual cingulum. It shares the same mesio-distal length and bucco-lingual width ratio with *Pongo* (1.05) (Pleistocene *Pongo* (ref. 14): 1.06, $N = 9$, range = 0.89–1.23), which is very different in *L. lufengensis* (ref. 17) (0.55–0.60). I_1 of *Pongo* is larger and has a stronger median lingual rib. The male lower canine is large with the base of its crown missing. Its cross-section is rounded, different from that of *L. lufengensis*. Its lingual wall bears two furrows, mesio-lingual and disto-lingual, bounding a strongly convex median vertical ridge. Canine shape and curvature are different from *L. lufengensis*, being more stout but more similar to that of Pleistocene *Pongo*¹⁴ and sharing a disto-buccal groove with *L. lufengensis*, *Griphopithecus* and *Pongo*. The male P_3 has no metaconid cusp. Its crown is less elevated and bucco-lingually wider with a more lingually slanted protoconid than that of *L. lufengensis* and there is no cingulid. DP_4 is molari-form with a small protoconid, resulting in a narrower mesial end and a strongly curved lingual surface, as in *Griphopithecus*. Its small and narrow trigonid is bent mesially and its paracristid has an arcuate shape as in *Pongo*¹⁸ and *Sivapithecus*². P_4 is similar to that of *L. lufengensis* but displays a longer talonid. It is slightly wider than long, has a lingually more slanted protoconid wall and its mesial part is wider than the distal. There is no cingulid, as on the lower molars, which are characterized by rounded and elevated cusps and strong enamel wrinkles. Measurements, from micro-computer tomography scans, of relative enamel thickness by Martin's method¹⁹ (Fig. 4) indicate values for male (17.23) and for female (17.80) M_2 that are closer to those obtained for an extant *Pongo pygmaeus* (16.52) and for *Pongo* mean (15.9) (ref. 20) rather than to *Griphopithecus* (19.7) (ref. 20). The morphology of the molars is similar to that of *L. lufengensis*, differing by their more slanted buccal walls and different M_3/M_2 proportions. M_3 size corresponds to that of the largest *L. lufengensis* M_3 s whereas M_2 size is in the middle of the *L. lufengensis* male range¹⁵. M_2 and M_3 have a short buccal cingulid. M_3 entoconid is extremely reduced and its hypoconulid is distally salient and centrally located. The lingual cusps and the hypoconulid of the lower molars have rounded horizontal wear facets, producing isolated and circular dentine pits similar to those of *L. lufengensis* which fuse together in late wear stages, unlike *Sivapithecus*.

To conclude, the new Thai species displays a strong resemblance to *Lufengpithecus*, but differs from it by several dental characters. *L. lufengensis* shows specialized characters in its anterior dentition: lower incisors are narrower mesio-distally, their crowns are higher, their length/width index is much smaller and their lower canine



Figure 4 Virtual vertical sections through the mesial cusps of M_2 of presumed male cf. *Lufengpithecus chiangmuanensis* (left) and extant *Pongo pygmaeus* (right) showing comparable relative enamel thickness and dentine penetration. Note also the stronger flaring of the buccal wall on the Thai fossil. Scale bar, 1 cm.

crowns are more elevated. Its skull^{21–23} and anterior teeth morphology exclude it from being a direct ancestor of orangutans. However, because cf. *L. chiangmuanensis* does not differ more profoundly in comparably preserved parts from *L. lufengensis*, but does appear to be the more closely related to *Pongo*, it might indeed be necessary, especially upon the discovery of more completely preserved specimens, to refer the new species to its own genus. However, pending these discoveries, *Lufengpithecus* would appear as a paraphyletic genus and therefore we propose to refer the new Thai species as cf. *Lufengpithecus chiangmuanensis* n. sp. Despite their more densely crenulated enamel and larger central incisors, Pleistocene and extant orangutans share many characters with cf. *L. chiangmuanensis* but display more derived features. *Sivapithecus* has some postcranial³ and skull characters¹ similar to those of *Pongo* but its dentition is less *Pongo*-like than that of the new Thai species. This new species is older than *L. lufengensis*, is known from the geographic area of Pleistocene *Pongo* and displays characters that make it the closest relative of extant *Pongo*. The dispersal corridor that we have identified, linking tropical Asia with Africa during the Middle Miocene, may also contribute to our understanding of Middle Miocene hominoid phylogeography. □

Methods

Chronology

Twenty-one oriented standard palaeomagnetic drill cores were collected from ten different stratigraphic levels. All samples were measured and analysed at the Laboratorio de Palaeomagnetismo, Universidad Nacional Autonoma de Mexico, on the JR5-A spinner magnetometer. Thermal and alternating fields were used for the demagnetization process. Thermal demagnetization of isothermal remanent magnetization (IRM) shows that magnetite and haematite are the main ferromagnetic minerals. Thermal demagnetization data for each specimen were generated from ten or more temperature steps (or six to nine alternating field steps), and then plotted on orthogonal vector diagrams to identify the characteristic remanent magnetization components (ChRM). The ChRM direction was calculated by using principal component analysis. Demagnetization isolates both normal and reverse polarities with an overall mean direction of $D = 9.8^\circ$, $I = 32.8^\circ$, $N = 14$ and $D = 175.9^\circ$, $I = -37.5^\circ$, $N = 5$, 20 out of 22 samples having been used for this analysis. The obtained data pass the analytical reversal test with 'C' quality classification. The mean direction is close to the expected direction derived from the apparent polar wander path of Eurasia, but the inclination value is lower than expected at the site latitude, consistent with a sedimentary inclination error for an original depositional remanent magnetization. This study highlights the succession of two normal polarities sandwiching a reverse polarity zone, the described hominoids originating from the upper normal zone (N2).

The large mammals are similar to those of the Chinji Formation of Pakistan (14–10.8 Myr). Mammalian fauna consists of stegolophodont mastodon, pig (*Hyotherium* cf. *pilgrimi*) and ruminants (*Eotragus*, *Dorcatherium* and *Siamotragulus*). The pig *H. pilgrimi* shows a temporal distribution in the Siwaliks between 14 and 11.3 Myr (J. Barry, personal communication). The tectonic phase affecting northern Thai intramontane basins is dated about 11.6 Myr (ref. 24). There are four possible correlations, requiring quite variable sedimentation rates through the section. The best fit, taking into account the estimated sedimentation rate²⁵ and the relative length of the reversals, suggests correlation with C5ABn chron corresponding to an age of 13.3–13.5 Myr for the upper normal polarity zone. But the chrons C5ABr and C5ABn are of nearly equal duration, and the sedimentation rate of N1 increases over that of R1. If we correlate R1 with chron C5AAr or chron C5Ar.1r and the corresponding normal chrons with C5AAn and C5An.2n, then it requires even greater differences in sedimentation rates. The last possible correlation is N2 with chron C5n.2n, and in that case, the youngest age for the level bearing cf. *L. chiangmuanensis* would be between 10 and 11 Myr. This age would correspond to the age of early hipparions, which appear in the Siwaliks at 10.7 Myr (ref. 9) and are present in the Late Miocene of Thailand, but absent from Chiang Muan. It appears less likely but still possible according to mammalian biochronology, but would imply a younger age as generally admitted for the tectonic event²⁴. Therefore, the combination of all the available data rather constrains the age of the new Thai hominoid to between 13.5 and 10 Myr.

Received 25 July 2002; accepted 17 January 2003; doi:10.1038/nature01449.

1. Pilbeam, D. New hominoid skull material from the Miocene of Pakistan. *Nature* **295**, 232–234 (1982).
2. Ward, S. in *Function, Phylogeny, and Fossils: Miocene Hominoid Evolution and Adaptations* (eds Begun, D. R., Ward, C. V. & Rose, M. D.) 269–290 (Plenum, New York, 1997).
3. Pilbeam, D., Rose, M. D., Barry, J. C. & Shah, S. M. I. New *Sivapithecus* humeri from Pakistan and the relationship of *Sivapithecus* and *Pongo*. *Nature* **348**, 237–239 (1990).
4. Wu, R. A revision of the classification of the Lufeng great apes. *Acta Anthropol. Sin.* **6**, 263–271 (1987).
5. Harrison, T., Ji, X. & Su, D. On the systematic status of the Late Neogene hominoids from Yunnan Province, China. *J. Hum. Evol.* **43**, 207–227 (2002).
6. Simons, E. L. & Chopra, S. R. K. *Gigantopithecus* (Pongidae, Hominoidea) A new species from north India. *Postilla* **138**, 1–18 (1969).
7. Kappelman, J. et al. in *Geology and Paleontology of the Sinap Formation* (eds Fortelius, M., Kappelman, J., Bernor, R. & Sen, S.) (Columbia University Press, New York, in press).

8. Alpagut, B., Andrews, P. & Martin, L. New hominoid specimens from the Middle Miocene site at Pasalar, Turkey. *J. Hum. Evol.* **19**, 397–422 (1990).
9. Barry, J. C. *et al.* Faunal and environmental change in the Late Miocene Siwaliks of northern Pakistan. *Paleobiology Memoirs* **3**(28), 1–71 (2002).
10. Morgan, M. E., Kingston, J. D. & Marino, B. D. Carbon isotopic evidence for the emergence of C4 plants in the Neogene from Pakistan and Kenya. *Nature* **367**, 162–165 (1994).
11. Cerling, T. E. *et al.* Global vegetation change through the Miocene/Pliocene boundary. *Nature* **389**, 153–158 (1997).
12. Pajunen, H. *Proc. Symp. Int. Peat Soc., Jamaica, 25 February–1 March 1985* (ed. Heikurainen, L.) 186–197 (Int. Peat Soc., Helsinki, 1985).
13. Badgley, C., Guoqing, Q., Wanyong, C. & Defen, H. Paleoeology of a Miocene, tropical, upland fauna: Lufeng, China. *Nat. Geogr. Res.* **4**, 178–195 (1988).
14. Hooijer, D. A. Prehistoric teeth of man and of the orang-utan from central Sumatra, with notes on the fossil orang-utan from Java and Southern China. *Zool. Med.* **29**, 175–301 (1948).
15. Kelley, J. & Plavcan, J. M. A simulation test of hominoid species number at Lufeng, China: implications for the use of the coefficient of variation in paleotaxonomy. *J. Hum. Evol.* **35**, 577–596 (1998).
16. Kelley, J., Anwar, M., McCollum, M. A. & Ward, S. C. The anterior dentition of *Sivapithecus parvada*, with comments on the phylogenetic significance of incisor heteromorphy in Hominoidea. *J. Hum. Evol.* **28**, 503–517 (1995).
17. Wu, R. & Oxnard, C. E. Ramapithecines from China: evidence from tooth dimensions. *Nature* **306**, 258–260 (1983).
18. Swarts, J. D. in *Orangutan Biology* (ed. Schwartz, J. H.) 263–270 (Oxford University Press, London, 1988).
19. Martin, L. Significance of enamel thickness in hominid evolution. *Nature* **314**, 260–263 (1985).
20. Martin, L. *The Relationships of the Later Miocene Hominoidea*. Thesis, Univ. London (1983).
21. Schwartz, J. H. in *Function, Phylogeny, and Fossils: Miocene Hominoid Evolution and Adaptations* (eds Begun, D. R., Ward, C. V. & Rose, M. D.) 363–388 (Plenum, New York, 1997).
22. Schwartz, J. H. *Lufengpithecus* and its potential relationship to an orang-utan clade. *J. Hum. Evol.* **19**, 591–605 (1990).
23. Harrison, T. & Rook, L. in *Function, Phylogeny, and Fossils: Miocene Hominoid Evolution and Adaptations* (eds Begun, D. R., Ward, C. V. & Rose, M. D.) 327–362 (Plenum, New York, 1997).
24. Remus, D., Webster, M. & Krawkan, K. Rift architecture and sedimentology of the Phetchabun intermontane basin, central Thailand. *J. Southeast Asian Earth Sci.* **8**, 421–432 (1993).
25. Johnson, N. M. & McGee, V. E. Magnetic polarity stratigraphy: stochastic properties of data, sampling problems, and the evolution of interpretations. *J. Geophys. Res.* **88**, 1213–1221 (1983).

Acknowledgements We thank P. Andrews, L. de Bonis, J. Kappelman, J. Kelley and D. Pilbeam for comments, help, discussion and providing comparative materials; J. H. Schwartz and J. Kappelman for improving our manuscript; E. Boller, J. Baruchel and the ID 19 beamline staff of the European Synchrotron Radiation Facility (Grenoble, France) for their help in obtaining microtomographic images; A. Sritulakarn and N. Wongchai for providing facilities in Chiang Muan coal mine; B. Marandat for preparing fossils and making casts; H. Tong for translating Chinese documents; J. Barry, P. Tassy, G. Métais and S. Ducrocq for identifying associated large mammals. This work was supported by the Wenner-Gren and the Fyssen Foundations, the Department of Mineral Resources (Bangkok) and TRF-CNRS Project.

Competing interests statement The authors declare that they have no competing financial interests.

Correspondence and requests for materials should be addressed to J.-J. (e-mail: jaeger@isem.univ-montp2.fr).

Species interactions can explain Taylor's power law for ecological time series

A. M. Kilpatrick & A. R. Ives

Department of Zoology, University of Wisconsin—Madison, Madison, Wisconsin 53706, USA

One of the few generalities in ecology, Taylor's power law^{1–3}, describes the species-specific relationship between the temporal or spatial variance of populations and their mean abundances. For populations experiencing constant per capita environmental variability, the regression of log variance versus log mean abundance gives a line with a slope of 2. Despite this expectation, most species have slopes of less than 2 (refs 2–4), indicating that more abundant populations of a species are relatively less variable than expected on the basis of simple statistical grounds. What causes abundant populations to be less variable has received

considerable attention^{5–12}, but an explanation for the generality of this pattern is still lacking. Here we suggest a novel explanation for the scaling of temporal variability in population abundances. Using stochastic simulation and analytical models, we demonstrate how negative interactions among species in a community can produce slopes of Taylor's power law of less than 2, like those observed in real data sets. This result provides an example in which the population dynamics of single species can be understood only in the context of interactions within an ecological community.

Taylor's power law describes the species-specific scaling relationship between the variance of population abundances and their means, which has been established for more than 400 species in taxa ranging from protists to vertebrates^{2,3}. The ubiquity of Taylor's power-law slopes of between 1 and 2 suggests an underlying fundamental explanation that might give insights into general ecological processes affecting many species. Furthermore, understanding the relationship between a population's variability and its mean abundance is needed to address numerous ecological problems, including conducting population viability analyses in conservation biology¹³, testing diversity–stability hypotheses^{14–16} and sampling for pests in agriculture^{17,18}.

There are two separate relationships between the variance and mean of a species's abundance, one temporal and one spatial³. Of these, the spatial relationship has received the most theoretical investigation^{5,7–12,19}. Here we focus on the temporal relationship in which the variance and mean abundance of a species through time are calculated for multiple populations, and these are graphed on a log–log scale with each datum representing a population. The null expectation for Taylor's power law for temporal variation is that the slope of the log variance versus log mean plot equals 2. This expectation derives from the well-known relationship that, when scaling any random variable X with finite mean μ and variance σ^2 by some constant k , the mean and variance of kX are $k\mu$ and $k^2\sigma^2$, respectively. On a log–log plot, the relationship between $k\mu$ and $k^2\sigma^2$ is a line with a slope of 2. A slope of less than 2 indicates that the per capita variability in population abundance decreases with increasing mean population abundance.

Taylor and others^{3,4} showed that the logarithm of the temporal variance of a population is tightly correlated to the logarithm of the mean abundance, with the correlation coefficient usually exceeding 0.9. For most species, the slope of the relationship is between 1 and 2. In an attempt to explain slopes of less than 2, Anderson and co-workers¹² showed that demographic stochasticity (variation caused by stochastic births and deaths of individuals in finite populations) in an exponentially growing population could lead to slopes for the temporal log variance versus log mean relationship of between 1 and 2, depending on the size of the population and the demographic parameters. Although demographic stochasticity certainly affects the dynamics of populations and can produce reduced slopes of Taylor's power law^{12,20,21}, these effects are most prevalent for population sizes on the order of hundreds or smaller. For many of the species considered by Taylor and others^{3,4}, the population size being sampled is likely to be in the tens of thousands or greater (for example, many insect species). For larger population sizes, environmental stochasticity in per capita population growth rates, which leads to a variance that scales with the square of the mean, overshadows the variance due to demographic stochasticity, which scales directly with the mean.

A second mechanism that could decrease the slope of Taylor's power law is sampling variance or error in the measurement of population abundance²². Sampling variance generally scales directly with the mean and thus by itself would produce a power-law slope of less than 2. Nevertheless, the effect of sampling variance on the slope declines with sampled abundance because at high abundance the variance–mean scaling will be dominated by environmental and/or demographic stochasticity. Although sampling variance certainly